Asymptotic normalization coefficients for $^{14}N+p\rightarrow{}^{15}O$ and the astrophysical S factor for $^{14}N(p,\gamma)^{15}O$

A. M. Mukhamedzhanov,[1] P. Bém,[2] B. A. Brown,[3] V. Burjan,[2] C. A. Gagliardi,[1] V. Kroha,[2] J. Novák,[2] F. M. Nunes,[3] Š. Piskoř,[2] F. Pirlepesov,[1] E. Šimečková,[2] R. E. Tribble,[1] and J. Vincour[2]

[1]*Cyclotron Institute, Texas A&M University, College Station, Texas 77843, USA*

[2]*Nuclear Physics Institute of Czech Academy of Sciences, Prague-Řež, Czech Republic*

[3]*National Superconducting Cyclotron Laboratory and Michigan State University, East Lansing, Michigan 48824, USA*

(Received 17 March 2003; published 20 June 2003; corrected 30 June 2003)

The $^{14}N(p,\gamma)^{15}O$ reaction, which controls energy production in the CNO cycle, has contributions from both resonance and direct captures to the ground and excited states. The overall normalization of the direct captures is defined by the corresponding asymptotic normalization coefficients (ANCs). Especially important is the ANC for the subthreshold state in ^{15}O at -0.504 keV since direct capture through this state dominates the reaction rate at stellar energies. In order to determine the ANCs for $^{14}N+p\rightarrow{}^{15}O$, the $^{14}N(^3He,d)^{15}O$ proton transfer reaction has been measured at an incident energy of 26.3 MeV. Angular distributions for proton transfer to the ground and five excited states were obtained. ANCs were then extracted from comparison to both distorted-wave Born approximation and coupled-channels Born approximation calculations. Using these ANCs, we calculated the astrophysical factor and reaction rates for $^{14}N(p,\gamma)^{15}O$. Our analysis favors a low value for the astrophysical factor.

DOI: 10.1103/PhysRevC.67.065804 PACS number(s): 26.20.+f, 21.10.Jx, 25.55.Hp, 27.20.+n

I. INTRODUCTION

The $^{14}N(p,\gamma)^{15}O$ reaction is one of the most important reactions in the CNO cycle. As the slowest reaction in the cycle, it defines the rate of energy production [1] and, hence, the lifetime of stars that are governed by hydrogen burning via CNO processing. Before 1987, the astrophysical factor for this reaction had been measured by several different groups (see Ref. [2] and references therein), but their results, extrapolated to zero energy, differed by about a factor of 2. Following an evaluation of the different experiments, Fowler *et al.* recommended the value of $S(0)\simeq 3.32$ keV b in their compilation [3]. In 1987, the $^{14}N(p,\gamma)^{15}O$ reaction was remeasured and results were obtained for transitions to the ground and excited states of ^{15}O. A total astrophysical factor $S(0)=3.20\pm 0.54$ keV b [2] was deduced, thus confirming the value recommended in Ref. [3]. These measurements led to a new understanding of the reaction, however, since it was found that $^{14}N(p,\gamma)^{15}O$ capture at low energies is dominated by resonant and direct capture to the first resonance at $E_R=259.5$ keV (the resonance energy in the center-of-mass system) and a subthreshold resonance at $E_s=-504$ keV. At very low energies appropriate for stellar burning, $E\rightarrow 0$, the reaction was found to be dominated by a combination of direct and resonant capture and interference from the tails of the subthreshold and first resonances.

A significant contribution to the total S factor, about 50%, came from resonance capture through the tail of the subthreshold state in the analysis of Schröder *et al.* [2]. In the analysis, they assumed a radiative width of 6.3 eV for the decay of the subthreshold resonance to the ground state. However, a recent new R-matrix analysis of their data by Angulo and Descouvemont [4] used a much smaller radiative width, which led to a significantly lower value for the total astrophysical factor, $S(0)=1.77\pm 0.2$ keV b. From their analysis, Angulo and Descouvemont determined that the dominant contribution to the total S factor at stellar energies comes from direct capture to the subthreshold state. The absolute normalization for the direct capture can be determined by its asymptotic normalization coefficient (ANC). In fact, Angulo and Descouvemont obtained an estimate for the ANC from their fit to the data at higher energies, and they noted that a measurement of this ANC was needed in order best to determine the low energy S factor. Very recently the first measurement of the radiative width of the subthreshold state in ^{15}O to the ground state was reported [5]. The new result for the width, $0.41^{+0.34}_{-0.13}$ eV, is about four times smaller than the value used by Angulo and Descouvemont and about 15 times smaller than the value used by Schröder *et al*. Consequently, the contribution to the S factor from resonance capture to the ground state through the subthreshold state in ^{15}O becomes negligible. The value of $S(0)$ that was reported in Ref. [5] agrees with the result of Angulo and Descouvemont [4] and is significantly lower than that of Ref. [2].

Here we report a new determination of the ANC for the subthreshold state at $\varepsilon=-504$ keV using the $^{14}N(^3He,d)^{15}O$ reaction at 26.3 MeV. Simultaneously, we have measured the ANCs for the ground and four other excited states in ^{15}O. We have also measured $^{14}N+{}^3He$ elastic scattering at the same energy to minimize the uncertainty in the extracted ANCs due to ambiguities in the entrance channel optical model parameters. Using the measured ANCs, we fit the astrophysical S factors for transitions to the ground and excited states and the total S factor using the R-matrix method. In our analysis, we accurately account for interference effects by splitting the resonance amplitudes into the internal and channel terms [6]. We find that for captures to all the states except the ground state, the $S(0)$ factors are almost entirely determined by the corresponding ANCs.

Recently similar measurements, but at a ^3He beam energy

of 20 MeV, have been reported [7]. Below we compare our extracted ANCs with this recent result. We also have carried out new, self-consistent, distorted-wave Born approximation (DWBA) and coupled-channels Born approximation (CCBA) calculations using both the data from Ref. [7] and our data in order to improve our knowledge of the ANCs for the subthreshold state.

II. EXPERIMENTAL DETAILS

The ANCs for $^{14}\mathrm{N}+p\rightarrow{}^{15}\mathrm{O}$ were determined from a comparison of the measured differential cross sections for the $^{14}\mathrm{N}(^{3}\mathrm{He},d)^{15}\mathrm{O}$ proton transfer reaction to a DWBA analysis. The angular distributions were measured at an incident ^{3}He beam energy of 26.3 MeV. The $^{14}\mathrm{N}(^{3}\mathrm{He},d)^{15}\mathrm{O}$ reaction has been studied by several groups but only relative cross sections were given for measurements at incident energies of 11 MeV [8] and 14 MeV [9]. In a recent measurement [10], only the transfer reaction between ground states was obtained. As we noted above, new measurements of absolute differential cross sections to both the ground and excited states in ^{15}O were performed recently by Bertone *et al.* [7], and ANCs were extracted. The experiment in Ref. [7] was carried out using a magnetic spectrometer to analyze the outgoing reaction products. They obtained very good energy resolution for the transfer reaction but had a rather large uncertainty in the normalization of the absolute cross section. The latter dominated the uncertainty in their results.

We have carried out an independent measurement of the absolute differential cross sections to both the ground and excited states in ^{15}O with the goal of determining the cross sections more accurately. We also measured $^{14}\mathrm{N}+{}^{3}\mathrm{He}$ elastic scattering concurrently in order to minimize uncertainties in the extracted ANCs due to ambiguities in the entrance-channel optical model potential. The experiment was carried out using a momentum analyzed 26.3-MeV ^{3}He beam from the U-120M isochronous cyclotron of the Nuclear Physics Institute of the Czech Academy of Sciences incident on a melamine ($C_3H_6N_6$) target. The initial thickness of the target was measured to be 260 ± 8 μg/cm^2 by scanning with well-collimated α-particle sources of ^{241}Am, ^{238}Pu, and ^{244}Cm. The target thickness was monitored continuously during the experiment by a Si detector telescope placed at a fixed angle $\theta_{lab}=19°$. Final states in four different reaction channels on ^{14}N—(^{3}He,p), (^{3}He,d), (^{3}He,^{3}He), and (^{3}He,^{4}He)—were observed in the monitor detector. A target thickness correction was then obtained for each angle from these measurements. The results were checked and found to be very consistent by measuring the same angle at several different times. Over the course of the experiment, the decrease in target thickness was $\sim$40%. Reaction products were observed by a pair of ΔE-E telescopes consisting of 250-μm-thick surface barrier detectors and 3000-μm-thick Si(Li) surface detectors. Both detectors subtended a solid angle of 0.23 msr. One telescope was fixed at $\theta_{LAB}=19°$ for monitoring purposes, while the other was rotated around the target and measured the reaction products at laboratory angles between 6.5° and 70°. The beam current was integrated by a Faraday cup biased to 800 V. Elastic scattering and spectra in several reaction channels were measured simultaneously by both telescopes to provide continuous calibration of the beam energy, reaction angle, and target thickness. Data were collected event by event in an external buffer and transferred to the online computer. Each data transfer also included information about the charge collected in the Faraday cup. Breaking the data into well defined blocks proved extremely valuable, as it allowed us to monitor the target thickness, which gradually decreased during the experiment. By accounting for the target thickness changes, it was possible to maintain a precision of $\pm4.4\%$ for the measured absolute differential cross sections. The experimental arrangement was similar to a previous measurement of $^{13}\mathrm{C}(^{3}\mathrm{He},d)\,^{14}\mathrm{N}$ [11].

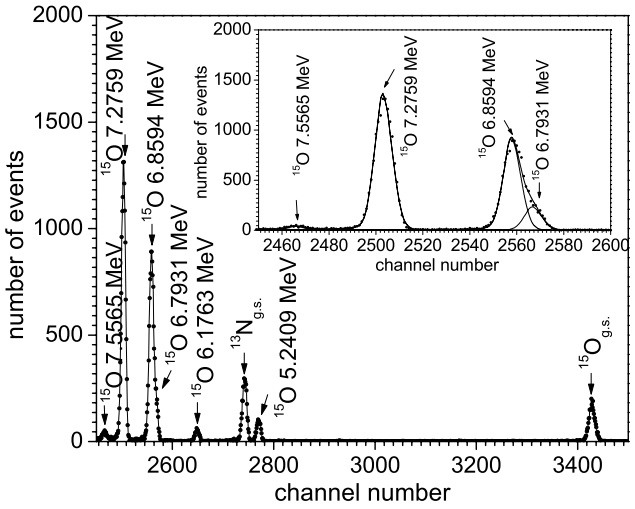

FIG. 1. Typical deuteron pulse height spectrum from the $^{14}\mathrm{N}(^{3}\mathrm{He},d)^{15}\mathrm{O}$ proton transfer reaction at 26.3 MeV, taken at a scattering angle $\theta_{LAB}=15.5°$. The deconvolution of the 6.79+6.86 MeV doublet in ^{15}O is presented in the inset.

The state of primary interest in our measurement was the subthreshold resonance state at an excitation energy of 6.79 MeV in ^{15}O. This is a member of a doublet with a separation energy of 66 keV. The average energy resolution for the outgoing d reaction products in our experiment was about 60 keV full width at half maximum. This was sufficient to deconvolute the doublet using both the line shape analysis from isolated nearby peaks and a precise energy calibration. This resolution also was enough to deconvolute the 5.2-MeV doublet, which includes the $1/2^+$, 5.18-MeV and $5/2^+$, 5.24-MeV states [12]. However, the combination of the line shape analysis and energy calibration indicated that only the 5.24-MeV state was populated. Figure 1 shows an example of a spectrum obtained in the present experiment, along with a fit to the 6.8-MeV doublet.

III. DATA ANALYSIS

In order to extract reliable ANCs, the analysis has been done using both DWBA and CCBA calculations with the FRESCO code [13]. The best optical potential in the entry channel, potential P_i in Table I, was obtained by fitting the ^{3}He elastic scattering angular distribution (see Fig. 2). For

TABLE I. The parameters of the Woods-Saxon optical model potentials used in the calculation of the ^{14}N(^{3}He, d)^{15}O proton transfer reaction. The parameters of the entry optical potential P_i have been extracted from the analysis of the ^{3}He+^{14}N elastic scattering data. The exit optical potential P_f is taken from Ref. [15].

Potential	V (MeV)	r_V (fm)	a (fm)	W_d (MeV)	r_d (fm)	a_d (fm)	V_{so} (MeV)	r_{so} (fm)	a_{so} (fm)	r_C (fm)
P_i	106.4	1.2624	0.6717	12.05	0.9227	1.0257				1.40
P_f	85.82	1.17	0.7346	12.2	1.325	0.6715	6.71	1.07	0.66	1.30

the output scattering channel, three different optical potentials, including the global parameters from Refs. [9,14,15], were used. We find that potential P_f [15], Table I, provides the best simultaneous fit for all the measured transitions. CCBA calculations allowed us to check for any channel-coupling effects [16]. To take into account coupling effects with other channels, the first three states of ^{14}N (1^+, $E_x=0.0$ MeV; 0^+, $E_x=2.313$ MeV; and 1^+, $E_x=3.948$ MeV) were included and coupled through a rotational model as in Ref. [16]. There is no experimental indication of deformation in ^{14}N. Consequently, we assumed a maximum value of $\beta_2=0.05$ to calculate the coupling strengths between these states. For ^{15}O, all six states presented in Table II were included in the calculation with $\beta_2=0.15$ [17]. No reorientation couplings were included, and both the real and imaginary parts of the interaction were deformed. In order to perform the CCBA calculations, the amplitudes for the various overlaps of the single particle states $\langle ^{14}\mathrm{N}_i|^{15}\mathrm{O}_j\rangle$ were also needed. These were obtained from shell model calculations within a p-sd shell space using WBP [18] for the p-shell and USD [19] for the sd shell. Single particle energies for the $d_{5/2}$ and $s_{1/2}$ levels were adjusted to the correct spacing given experimentally by the ^{17}F spectrum [12]. We find that channel coupling effects are not important in this reaction and the DWBA cross sections are modified by only $\approx 1\%$ for all the final states.

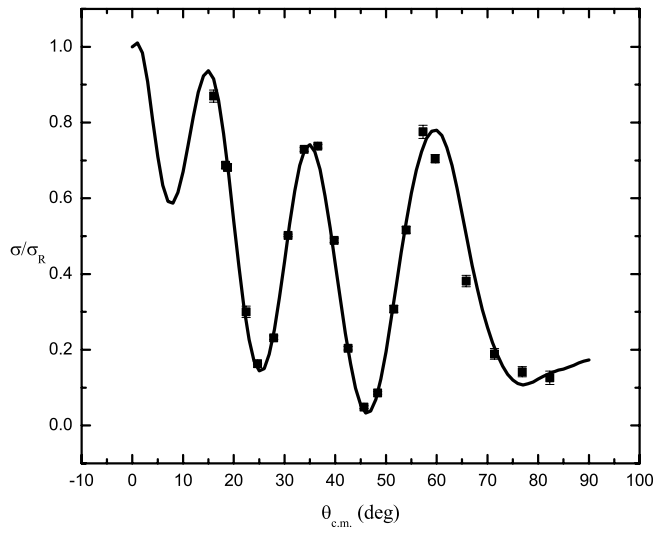

FIG. 2. Measured elastic scattering angular distribution for ^{14}N+^{3}He at 26.3 MeV, and the fit using optical potential P_i from Table I. Statistical uncertainties for most data points are smaller than the size of the dots that show the data.

Angular distributions of deuterons from the ^{14}N (^{3}He, d) ^{15}O reaction leading to the most important transitions, the ground, third, fourth, and fifth excited states in ^{15}O, together with DWBA fits using the parameters in Table I, are shown in Fig. 3. For the transition to the fourth excited state, which is the most important for nuclear astrophysics, we also show our DWBA fit to the measurement reported in Ref. [7]. The ANCs were determined by normalizing the calculated DWBA differential cross sections to the experimental ones.

For all the ^{15}O final states, the calculations have been checked to verify that the transitions are peripheral. Hence, by normalizing the DWBA calculations to the data in the region of the main maximum of the angular distributions and using a well known value of the ANC for $^{3}\mathrm{He}\rightarrow d+p$ [20] ($C^2=3.90\pm 0.06$ fm^{-1}), the ANCs for $^{14}\mathrm{N}+p\rightarrow{}^{15}\mathrm{O}$ can be determined. The extracted ANCs are given in the third column of Table II. For comparison, in the last column we present the ANCs determined in Ref. [7]. The uncertainties, which are discussed below, take into account experimental uncertainties and uncertainties due to ambiguity in the optical model parameters for the initial and final states.

The proton transfer reaction to the ground and 6.18-MeV states in ^{15}O can populate both $p_{1/2}$ and $p_{3/2}$ orbitals. We cannot separate these contributions because the (^{3}He,d) reaction is insensitive to the value of the total angular momentum of the transferred proton, so we measure their sum. The DWBA cross section for the transfer to the ground state has been calculated using the ratio of the spectroscopic factors $S_{3/2}/S_{1/2}=0.10$ given by shell-model calculations using the OXBASH code [21]. The overall uncertainty of the extracted ANCs is 11%. The main contributions were the uncertainty in absolute normalization of the experimental angular distributions (4.5%) and the uncertainty due to ambiguity in the optical model parameters for both the initial and final channels (10%). Only the second state of the 5.2-MeV doublet has been identified in our experiment, and we determined the ANC for that state with a total uncertainty of 11% (see Table II). For the transition to the third excited state, $E_x=6.18$ MeV, we use the shell-model prediction indicating that the population of the $p_{3/2}$ component is negligible compared to the $p_{1/2}$ component. We assign a total uncertainty of 12% for $C^2_{p_{1/2}}$. The most important transition, and the most difficult to analyze, is the transfer reaction to the $3/2^+$, 6.79 MeV, fourth excited state. Here $s_{1/2}$, $d_{3/2}$, and $d_{5/2}$ orbitals all contribute. In the analysis we used the ratio of the spectroscopic factors predicted by the shell-model calculation, $(d_{3/2})/(d_{5/2})/(s_{1/2})=(0.014)/(0.027)/(0.734)$. Note that a variation in the relative contributions of the d wave and s

TABLE II. The ANCs for $^{14}N+p\rightarrow{}^{15}O$. J_f^π, E_f, are the spin parities and the excitation energies of the states in ^{15}O, given in the first column; the corresponding proton orbital and total angular momenta, l_f and j_f, are given in the second column. The ANCs (in fm^{-1}) determined here from the $^{14}N(^3He,d)^{15}O$ reaction are given in the third column, and those from Ref. [7] are given in the fourth column.

State ^{15}O	Proton orbitals	ANC	
J_f^π, E_f (MeV)	l_{fj_f}	C^2 (fm^{-1})	C^2 (fm^{-1})
$1/2^-$, 0.00	$p_{1/2}$	49.0 ± 5.4	63 ± 14[a]
	$p_{3/2}$	5.00 ± 0.55	
$5/2^+$, 5.24	$d_{5/2}$	0.11 ± 0.01	0.12 ± 0.03
$3/2^-$, 6.18	$p_{1/2}$	0.50 ± 0.06	0.46 ± 0.10
$3/2^+$, 6.79	$s_{1/2}$	24.0 ± 5.0	
	$d_{3/2}$	0.006 ± 0.001	
	$d_{5/2}$	0.01 ± 0.002	
$3/2^+$, 6.79	$s_{1/2}$	27.1 ± 6.8[b]	21 ± 5
	$d_{3/2}$	0.006 ± 0.002[b]	
	$d_{5/2}$	0.01 ± 0.003 [b]	0.080 ± 0.020
$5/2^+$, 6.86	$d_{5/2}$	0.32 ± 0.04	0.36 ± 0.08
$7/2^+$, 7.27	$d_{5/2}$	$(2.35\pm0.18)\times10^6$	$(2.7\pm0.6)\times10^6$

[a]The sum $C^2_{p_{1/2}}+C^2_{p_{3/2}}$.
[b]The ANC determined by us from the data in Ref. [7].

wave does little to change the quality of the fit but introduces an additional uncertainty of ~18% in the extracted ANC. However, this kind of uncertainty has not been considered here due to reliance on the shell-model code. We find that the ANC is quite sensitive to the exit channel optical potential. By modifying the exit channel, we can obtain an improved fit for this transition, but the modified potential fails to reproduce the angular distributions for transitions to other bound states, and, in particular, the ground state. Consequently, we assign a 20% uncertainty to the ANC for the $3/2^+$, 6.79-MeV state due to the ambiguity of the optical potential parameters. Taking into account the experimental uncertainty, we obtain 21% as the overall uncertainty of the ANC $C^2_{s_{1/2}}$.

Since this ANC plays a crucial role in the determination of the rate of ^{15}O formation, we also reanalyzed the data from Ref. [7] in a manner consistent with that used in this work. Since the uncertainty in the cross-section normalization in Ref. [7] is 14.5%, three times as high as that of the present measurement, we assign a higher uncertainty of 25% to the ANCs determined from the analysis of those data for the transition to $3/2^+$, 6.79-MeV state. From Table II it is clear that the values for the primary ANC, $C_{s_{1/2}}$, determined from the two recent experiments agree quite well and overlap with the the ANC obtained in Ref. [7]. The primary difference between the two analyses is due to how the different relative contributions of the *s* and *d* orbitals were determined. We used the relative weights predicted by the shell model, whereas in Ref. [7], this value was a fitting param-

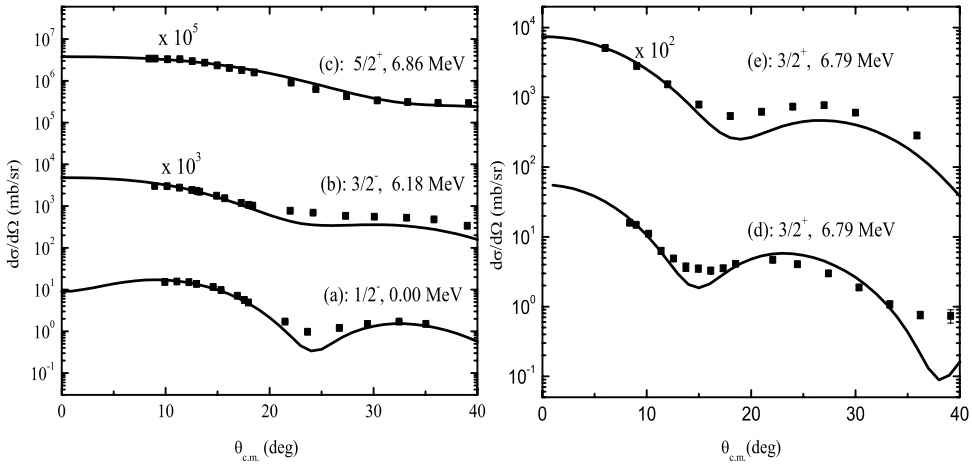

FIG. 3. The $^{14}N(^3He,d)^{15}O$ differential cross sections. The squares are data points and the solid lines are the DWBA calculations normalized to the experimental measurements in the main peaks. The transitions are to states in ^{15}O at (a) $1/2^-$, 0.00 MeV; (b) $3/2^-$, 6.18 MeV; (c) $5/2^+$, 6.86 MeV; (d) $3/2^+$, 6.79 MeV; and (e) $3/2^+$, 6.79 MeV (our fit of the angular distribution measured in Ref. [7]). Statistical uncertainties for most data points are smaller than the size of the dots that show the data.

eter. The result in Ref. [7] shows a significantly higher contribution from the *d* orbital than the shell-model prediction. Clearly, an independent determination of the contributions from the two orbitals to this state would help in reducing the overall uncertainty in this ANC.

IV. RESULTS AND DISCUSSION

To calculate the astrophysical factors we used the *R*-matrix approach [6]. The subthreshold *s*-wave bound state plays a crucial role in the determination of the astrophysical $S(0)$ factor in two ways. As a bound state it gives a contribution to resonance capture (through the $1/2^+$, 7.56-MeV resonance) and direct capture. As a subthreshold resonance, it can contribute to the resonance capture to the ground and low-lying states. In the *R*-matrix approach the normalization of the direct capture amplitude is governed by the ANC of the final bound state [6]. All direct capture contributions are considered to be $E1$ transitions. The convolution of our fits with the target thickness has not been done here, because it affects only the fits in the resonance area and does not affect the $S(E)$ factors at small energies. Fits were actually done by eliminating the points near the resonance because of this problem.

The capture rate to the ground state has been difficult to determine due to the uncertainty in the resonance contribution to the ground state through the subthreshold state at 6.79 MeV. This resonance amplitude interferes with direct capture to the ground state with channel spin $I=3/2$ and the second resonance at 8.284 MeV, which is also a $3/2^+$ *s*-wave resonance. To obtain a reasonable fit to the experimental data [2], a contribution from a background pole generated by distant resonances must also be taken into account. Furthermore, the first resonance interferes with the channel spin $I=1/2$ direct term. There are two important characteristics of the subthreshold resonance: its proton partial width and the radiative width for the decay to the ground state, which has been determined in Ref. [5]. According to previous work [22], the proton partial width of the subthreshold resonance can be expressed in terms of the ANC for this state. By measuring this ANC we have determined the proton partial width, which was a missing characteristic of the subthreshold resonance needed to determine the *S* factor. Also, the channel radiative width at zero energy can be found from the measured ANC for the decay of the subthreshold resonance to the ground state [6].

For a channel radius $r_0=5.5$ fm and the value of the ANC, $C^2=25.5$ fm^{-1}, the resulting channel radiative width is $\Gamma_{\gamma ch}(E=0)=0.79$ eV. Using this value we can determine the internal radiative width. We assume a value of the total radiative width, $\Gamma_\gamma(E=0)=0.35$ eV, which provides the best fit and is consistent with the value measured in Ref. [5]. Using the relationship $\Gamma_\gamma(E)=|\Gamma^{1/2}_{\gamma ch}(E)-\Gamma^{1/2}_{\gamma int}(E)|^2$, we find for the internal radiative width $\Gamma_{\gamma int}(E=0)=0.09$ eV. The imaginary part of $\Gamma^{1/2}_{\gamma ch}(0)$ is negligibly small.

The *S*-factor fit for the transition to the ground state is displayed in Fig. 4(a). Its uncertainty is dominated by the uncertainty in the ANCs for the ground state and the $3/2^+$, 6.79-MeV subthreshold resonance in ^{15}O, $\sim$30% uncertainty due to the uncertainty of the *R*-matrix channel radius, experimental uncertainty in the radiative width for the decay of the subthreshold resonance to the ground state [5], and the 13% systematic uncertainty in the experimental $S(E)$ factor [2]. We find that the astrophysical factor for the capture to the ground state is $S(0)=0.15\pm0.07$ keV b, which is significantly lower than the value $S(0)=1.55\pm0.34$ keV b found in Ref. [2] and agrees with the value $S(0)=0.08^{+0.13}_{-0.06}$ keV b determined in Ref. [4]. Only the direct capture $S(0)$ factor for the transition to the ground state is given in [7]. Note that the direct capture term alone is significantly higher than $S(0)$, but it is suppressed by interference with the resonant terms.

The capture to the $3/2^-$, 6.18-MeV third excited state is similar to the capture to the ground state. It has a contribution from direct capture and resonance captures through the first, second, subthreshold, and background resonances. The radiative width for the decay of the subthreshold resonance to the third excited state has not been measured. We assume for this width a value of 30.0 meV at $E=0$. This corresponds to 5.0 meV at $E_s=-0.504$ MeV, which is in the range of the radiative width, 5.0 ± 3.0 meV, determined in Ref. [4] from the fit. The channel and internal widths for the decay of the subthreshold resonance to the third excited state are $\Gamma_{\gamma ch}(E=0)=3.0$ meV and $\Gamma_{\gamma int}(E=0)=53.0$ meV, respectively. The calculated $S(0)$ astrophysical factor for the capture to the third excited state is $S(0)=0.13\pm0.02$ keV b. Its uncertainty is determined by the uncertainties of the parameters of the resonances, the 12% uncertainty in the ANC for the third excited state in ^{15}O, and the 13% systematic uncertainty in the experimental $S(E)$ factor [2]. The variation of the channel radius by 20% changes $S(0)$ by only 2.5%. The calculated and experimental $S(E)$ factors for the transition to the third excited state are presented in Fig. 4(b).

Capture to the $3/2^+$, 6.79-MeV, subthreshold state has contributions from resonance capture through the first resonance and direct $E1$ capture, which do not interfere. $E2$ direct capture to the 6.79-MeV state contributes significantly less than 1% of the dominant $E1$ capture. Due to the very small binding energy of the 6.79-MeV state, direct capture to this state is extremely peripheral and the low-energy $S(E)$ factor is practically insensitive to the value of the channel radius. For example, a change of the channel radius by 20% changes the $S(0)$ factor only by 1.3%. This uncertainty has also been taken into account. The capture to this state dominates all others and the calculated astrophysical factor is $S(0)=1.40\pm0.20$ keV b. The uncertainty in $S(0)$ is entirely determined by the ANC of this state and the 13% systematic uncertainty in the experimental $S(E)$ factor [2]. The calculated and experimental $S(E)$ factors for the transition to this subthreshold state are presented in Fig. 4(c).

The last two subthreshold states, $5/2^+$, 6.86 MeV and $7/2^+$, 7.28 MeV, provide contributions only by direct capture at energies <500 keV [2]. Due to the small binding energy, both captures are extremely peripheral and their overall normalization and uncertainties are defined by the corresponding ANCs and their uncertainties. The astrophysical factor

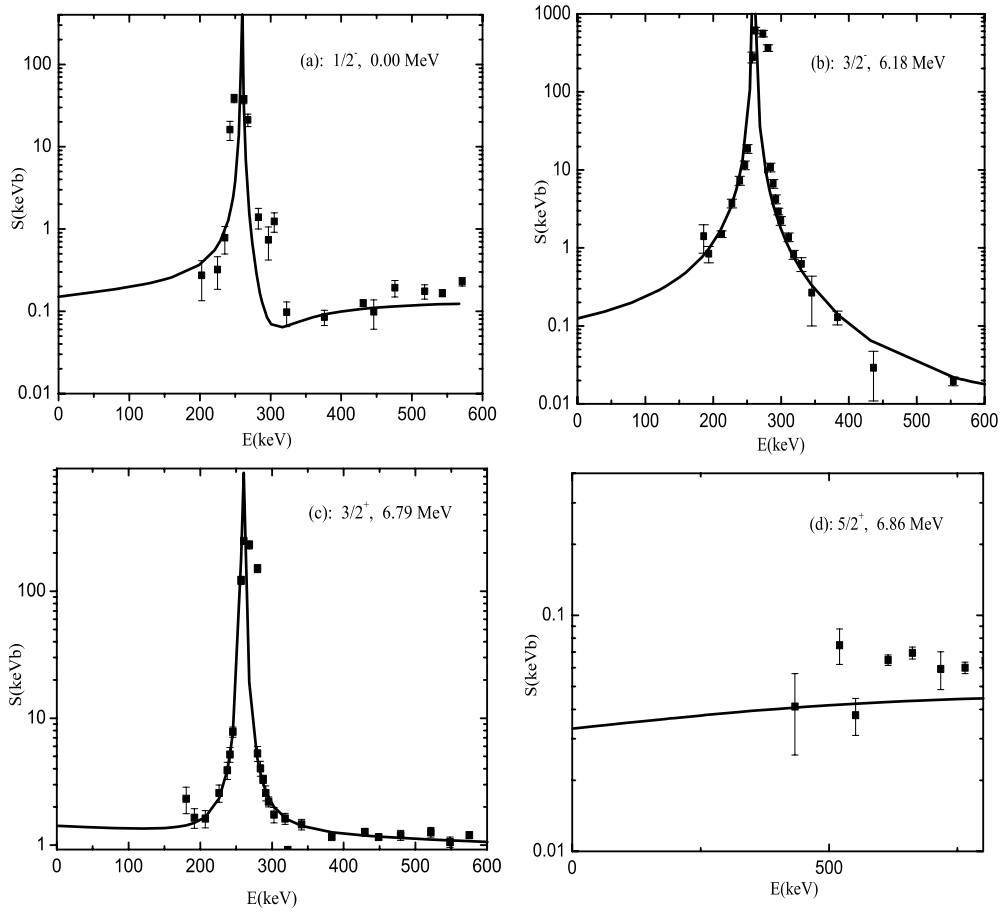

FIG. 4. The $^{14}\mathrm{N}(p,\gamma)^{15}\mathrm{O}$ astrophysical S factors. The squares are data points [2]; the solid lines represent the calculated S factors (best fit). For captures to the ground state [(a) $1/2^-$, 0.00 MeV] and to the third excited state [(b) $3/2^-$, 6.18 MeV], it includes the resonant and nonresonant capture terms and their interference. For capture to the fourth excited state [(c) $3/2^+$, 6.79 MeV], it includes the incoherent sum of the resonant and nonresonant terms, and for capture to the fifth excited state [(d) $5/2^+$, 6.86 MeV], the calculated S factor includes only direct capture term.

TABLE III. The low-energy astrophysical factors and low-temperature reaction rates for $^{14}\mathrm{N}+p\rightarrow{}^{15}\mathrm{O}+\gamma$. First and second columns: energy in keV and astrophysical $S(E)$ factor in keV b. The third and fifth columns: temperature in T_9. The fourth and sixth columns: our adopted reaction rates in $\mathrm{cm}^3\ \mathrm{mol}^{-1}\ \mathrm{s}^{-1}$. The values in square brackets denote powers of 10.

E (keV)	$S(E)$ (keV b)	Temperature (T_9)	Rate ($\mathrm{cm}^3\ \mathrm{mol}^{-1}\ \mathrm{s}^{-1}$)	Temperature (T_9)	Rate ($\mathrm{cm}^3\ \mathrm{mol}^{-1}\ \mathrm{s}^{-1}$)
1	1.73	0.007	1.9 [-26]	0.035	1.5 [-12]
30	1.74	0.008	5.6 [-25]	0.040	1.1 [-11]
50	1.75	0.009	9.8 [-24]	0.045	5.4 [-11]
70	1.77	0.010	1.1 [-22]	0.050	2.2 [-10]
100	1.83	0.011	9.8 [-22]	0.055	7.6 [-10]
120	1.89	0.012	6.5 [-21]	0.060	2.3 [-09]
140	1.99	0.013	3.6 [-20]	0.065	6.0 [-09]
160	2.16	0.014	1.7 [-19]	0.070	1.4 [-08]
180	2.47	0.015	6.6 [-19]	0.075	3.2 [-08]
200	3.15	0.016	2.4 [-18]	0.080	6.6 [-08]
210	3.82	0.018	2.2 [-17]	0.085	1.3 [-07]
225	6.07	0.020	1.6 [-16]	0.090	2.4 [-07]
235	10.29	0.025	7.5 [-15]	0.095	4.2 [-07]
243	20.34	0.030	1.4 [-13]	0.100	7.2 [-07]

for capture to the $5/2^+$, 6.86-MeV state is $S(0)=0.03 \pm 0.04$ keV b. The calculated and experimental $S(E)$ factors for the transition to this state are presented in Fig. 4(d). According to Ref. [2], the captures to the 5.2-MeV doublet and to the $7/2^+$, 7.28-MeV state contribute about 3% to the total $S(0)$ factor and have been neglected here.

The total calculated astrophysical factor at zero energy is $S(0)=1.70\pm0.22$ keV b. Note that the uncertainty of the total $S(0)$ factor is essentially determined by the uncertainty in the ANC for the subthreshold bound state at 6.79 MeV. Thus we confirm the low value of the $S(0)$ factor reported in Refs. [4,7]. Several early measurements of the S factor are not consistent with more recent results [2,5]. In particular, the low-energy $S(E)$ measured using β^+ activity from ^{15}O [23] does not agree with the low-energy $S(E)$ obtained by the extrapolation of the experimental data from Ref. [2] using the value of the radiative width of the subthreshold resonance at 6.79 MeV measured in Ref. [5]. Also, measurements of direct capture $S(0)$ factors for transitions to 6.18- and 6.79-MeV states were reported in Ref. [24] but the large value reported for the 6.18-MeV level is completely inconsistent with recent results and ANCs for this state determined in the present work and in Ref. [7]. Consequently, we restricted the analysis used here to the experimental data from Ref. [2].

Our low-energy astrophysical factor and low-temperature reaction rates are given in Table III. The uncertainty in the $S(E)$ factors and the reaction rates is 21%. Our reaction rates are very close to those calculated in Ref. [4] and confirm a significantly lower production rate of ^{15}O than was obtained previously [3,2]. They are also smaller than the reaction rates recommended by NACRE [25]. For the temperature interval $T_9=0.007-0.1$, where T_9 is the temperature in 10^9 K, our adopted reaction rates differ from the NACRE rates by 84–54 %.

Massive main sequence stars, especially at the end of their life, and red giants generate energy via the CNO cycle. ^{14}N$(p,\gamma)^{15}$O, as a bottleneck reaction of the cycle, controls the rate of the CNO-cycle energy production. Hence the ^{14}N$(p,\gamma)^{15}$O rate affects stellar structure and evolution, such as the luminosity at the transition period from the main sequence to the red giants, which is used to determine the ages of globular clusters [5,26] and serves as a diagnostic of the stellar interior [27]. It also affects nucleosynthesis in the red giants beyond the CNO cycle [5]. The impact of the low rates of the ^{14}N$(p,\gamma)^{15}$O on different astrophysical characteristics is discussed in Ref. [5]. In particular, the lower reaction rates lead to an increase in the age of the main-sequence turnoff in globular clusters [5].

ACKNOWLEDGMENTS

This work was supported in part by the U.S. Department of Energy under Grant No. DE-FG03-93ER40773, the U.S. National Science Foundation under Grant Nos. INT-9909787, PHY-0140343, and PHY-007091, ME 385(2000) project NSF and MSMT, CR, Grant No. GACR 202/01/0709, by the Grant No. POCTI/36282/99 (Portugal), and by the Robert A. Welch Foundation.

[1] C. Rolfs and W. S. Rodney *Cauldrons in the Cosmos* (The University of Chicago Press, Chicago, 1988).
[2] U. Schröder *et al.*, Nucl. Phys. **A467**, 240 (1987).
[3] W.A. Fowler, G.R. Caughlan, and B.A. Zimmerman, Annu. Rev. Astron. Astrophys. **13**, 69 (1975).
[4] C. Angulo and P. Descouvemont, Nucl. Phys. **A690**, 755 (2001).
[5] P.F. Bertone, A.E. Champagne, D.C. Powell, C. Iliadis, S.E. Hale, and V.Y. Hansper, Phys. Rev. Lett. **87**, 152501 (2001).
[6] F.C. Barker and T. Kajino, Aust. J. Phys. **44**, 369 (1991).
[7] P.F. Bertone, A.E. Champagne, M. Boswell, C. Iliadis, S.E. Hale, V.Y. Hansper, and D.C. Powell, Phys. Rev. C **66**, 055804 (2002).
[8] W. Bohne, H. Homeyer, H. Morgenstern, and J. Scheer, Nucl. Phys. **A113**, 97 (1969).
[9] W.P. Alford and K.H. Purser, Nucl. Phys. **A132**, 86 (1969).
[10] S.V. Artemov, I.R. Gulamov, E.A. Zaparov, I.Y. Zotov, and G.K. Nie, Yad. Fiz. **59**, 454 (1996) [Phys. At. Nucl. **59**, 428 (1996)].
[11] P. Bem, V. Burjan, V. Kroha, J. Novak, S. Piskor, E. Simeckova, J. Vincour, C.A. Gagliardi, A.M. Mukhamedzhanov, and R.E. Tribble, Phys. Rev. C **62**, 024320 (2000).
[12] F. Ajzenberg-Selove, Nucl. Phys. **A449**, 1 (1986).
[13] I.J. Thompson, Comput. Phys. Rep. **7**, 167 (1988).
[14] C.M. Perey and F.G. Perey, At. Data Nucl. Data Tables **17**, 1 (1976).
[15] W.W. Daehnick, J.D. Childs, and Z. Vrcelj, Phys. Rev. C **21**, 2253 (1980).
[16] F.M. Nunes and A.M. Mukhamedzhanov, Phys. Rev. C **64**, 062801(R) (2001).
[17] V. Burjan, J. Cejpek, J. Fojtu, V. Kroha, D.V. Aleksandrov, V.G. Novatskii, and D.N. Stepanov, Z. Phys. A **354**, 281 (1996).
[18] E.K. Warburton and B.A. Brown, Phys. Rev. C **46**, 923 (1992).
[19] B.A. Brown and B.H. Widenthal, Annu. Rev. Nucl. Part. Sci. **38**, 29 (1988).
[20] A.M. Mukhamedzhanov, R.E. Tribble, and N.K. Timofeyuk, Phys. Rev. C **51**, 3472 (1995).
[21] B. A. Brown, A. Etchegoyen, and W. D. M. Rae, MSU-NSCL Report No. 524 (1988).
[22] A.M. Mukhamedzhanov and R.E. Tribble, Phys. Rev. C **59**, 3418 (1999).
[23] W.A.S. Lamb and R.E. Hester, Phys. Rev. **108**, 1304 (1957).
[24] D.F. Hebbard and G.M. Bailey, Nucl. Phys. **49**, 666 (1963).
[25] C. Angulo *et al.*, Nucl. Phys. **A656**, 3 (1999).
[26] D.A. VandenBerg, M. Bolte, and P.B. Stetson, Astron. J. **100**, 445 (1990).
[27] S.A. Becker and I. Iben, Astrophys. J. **232**, 831 (1979).